Tectonophysics 637 (2014) 178–190

Contents lists available at ScienceDirect

Tectonophysics

journal homepage: www.elsevier.com/locate/tecto

Paleoseismology of the 2010 M_w 7.1 Darfield (Canterbury) earthquake source, Greendale Fault, New Zealand

S. Hornblow [a,*], M. Quigley [a], A. Nicol [b], R. Van Dissen [b], N. Wang [c]

[a] Department of Geological Sciences, University of Canterbury, Christchurch, New Zealand
[b] GNS Science, Lower Hutt, New Zealand
[c] School of Geography, Environment and Earth Sciences, Victoria University of Wellington, Wellington, New Zealand

A R T I C L E I N F O

Article history:
Received 2 June 2014
Received in revised form 17 August 2014
Accepted 3 October 2014
Available online 16 October 2014

Keywords:
Paleoearthquakes
Ground surface rupture
Strike slip displacements
Darfield earthquake

A B S T R A C T

The previously unknown Greendale Fault ruptured in the September 2010 moment magnitude (M_w) 7.1 Darfield Earthquake. Surface rupture fracture patterns and displacements along the fault were measured with high precision using real time kinematic (RTK) GPS, tape and compass, airborne light detection and ranging (lidar), and aerial photos. No geomorphic evidence of a penultimate surface rupture was revealed from pre-2010 imagery. The fault zone is up to 300 m wide and comprises both distributed (folding) and discrete (faulting) deformation dominated by right-lateral displacement. Surface fracturing accommodates ~30% of the total right-lateral displacement in the central fault zone; the remainder is accommodated by distributed deformation. Ground penetrating radar and trenching investigations conducted across the central Greendale Fault reveal that most surface fractures are undetectable at depths exceeding 1 m; however, large, discrete Riedel shears continue to depths exceeding 3 m and displace interbedded gravels and sand-filled paleochannels. At one trench site, a Riedel shear displaces surface agricultural markers (e.g., fences and plow lines) and a subsurface (0.6 m deep) paleochannel by 60 cm right-laterally and 10 cm vertically, indicating the paleochannel has been displaced only in the Darfield earthquake. Optically stimulated luminescence (OSL) dating of the displaced paleochannel yields an age of 21.6 ± 1.5 ka. Two additional paleochannels at ~2.5 m depth with OSL ages of 28.4 ± 2.4 ka and 33 ± 2 ka have been displaced ~120 cm right-laterally and ~20 cm vertically. The doubling of displacement at depth is interpreted to indicate that in the central section of the Greendale Fault the penultimate surface-rupturing event occurred between ca. 20 and 30 ka. The Greendale Fault remained undetected prior to the Darfield earthquake because the penultimate fault scarp was eroded and buried during Late Pleistocene alluvial activity. Similar active faults with low slip rates (i.e. lower than sedimentation/erosion rates) are likely to be concealed in alluvial settings globally.

1. Introduction

Despite significant scientific advances in the detection and mapping of active faults worldwide, many historical earthquakes have caused surface rupture on faults that were previously unknown due to a paucity or absence of evidence of prior surface rupture. Recent examples include the 2001 Bhuj (India) M_w 7.7 (McCalpin and Thakkar, 2003), 2010 El Cucapah M_w 7.2 (Oskin et al., 2012), and the 2010 Darfield (Canterbury) M_w 7.1 earthquakes (Quigley et al., 2010a, 2010b). Characterizing the earthquake history of previously undetected faults and understanding why they evaded detection is important for assessing the completeness of active fault catalogues contributing to seismic hazard models. It is also important for understanding the maximum earthquake M_w potential for areas where surface rupturing faults have not been identified (e.g., Stirling et al., 2012).

Sedimentation or erosion may obscure or remove evidence for surface faulting in alluvial settings and increase the challenge of detecting active faults. Strike-slip faults with typically low-relief rupture traces are particularly susceptible to burial or erosion. Undersampling of active faults at the ground surface is exacerbated when fault slip rates are slow relative to the rates of surface processes (e.g., Gold et al., 2013). Fault detection is likely to be most difficult at the peripheries of active plate boundary zones, where rapid rates of surface processes due to proximal orogenic activity may overlap with areas of lower strain rates and longer earthquake recurrence intervals. Furthermore, when rupture occurs through thick packages of unconsolidated sediments, the total displacement may be expressed as a combination of discrete surface faulting and broad wavelength folding (Quigley et al., 2012; Van Dissen et al., 2011), with the latter typically difficult to recognize in the geologic record (Bray and Kelson, 2006; Fielding et al., 2009; Oskin et al., 2012; Rockwell and Klinger, 2013; Rockwell et al., 2002; Wesnousky, 2008). For this reason, the use of displaced geomorphic features to estimate the slip and M_w of paleoearthquakes relies upon the careful documentation of single-event

* Corresponding author.
E-mail address: sharon.hornblow@pg.canterbury.ac.nz (S. Hornblow).

http://dx.doi.org/10.1016/j.tecto.2014.10.004

coseismic slip and slip variability from historic earthquakes for which slip and M_w were recorded (e.g., Wells and Coppersmith, 1994; Wesnousky, 2008). Discrete surface ruptures typically account for 50–60% of the slip of their subsurface equivalent (e.g., Dolan and Haravitch, 2014).

The 2010 M_w 7.1 Darfield (Canterbury) earthquake triggered the 2010–2011 Canterbury earthquake sequence, which includes three earthquakes of M_w 6 or greater (Bannister and Gledhill, 2012). The 22 February 2011 M_w 6.2 Christchurch earthquake caused 185 fatalities and the greatest damage (e.g., Bradley et al., 2014; Kaiser et al., 2012) (Fig. 1). Of the faults that accrued slip during the Canterbury earthquake sequence only the Greendale Fault generated ground-surface rupture (Figs. 1 and 2A) (Beavan et al., 2012; Elliott et al., 2012; Quigley et al., 2010a, 2010b). The Greendale Fault surface rupture morphology and associated coseismic displacements have been extensively studied using combined field, lidar, InSAR, and geodetic techniques (Barrell et al., 2011; Duffy et al., 2013; Elliott et al., 2012; Litchfield et al., 2014a; Quigley et al., 2012; Van Dissen et al., 2011, 2013; Villamor et al., 2011, 2012). Abandoned river meanders and terrace patterns have been tentatively interpreted to suggest fault-related pre-2010 Holocene uplift at the western end of the Greendale Fault (Campbell et al., 2012). However, neither interpretation of ortho-photographs predating the Darfield earthquake nor analysis of post-Darfield imagery provides unequivocal evidence that the Greendale Fault ruptured the ground surface prior to 2010 (Villamor et al., 2012). In the absence of a clear pre-2010 surface trace, sub-surface information is required to constrain the paleoearthquake history of the fault. The Greendale Fault paleoseismic history has not been studied prior to this investigation.

This paper summarizes the tectonic, geologic and geomorphic setting of the Greendale Fault together with the surface rupture morphology and displacements obtained from the fault trace following the Darfield earthquake. New ground penetrating radar (GPR) and trenching data from two sites on the central Greendale Fault constrain the subsurface fault geometry and displacements. The timing of the penultimate event in the trenches has been constrained by new optically stimulated luminescence (OSL) dating of faulted stratigraphic units. Our results illuminate some of the challenges of detecting and studying active faults in alluvial landscapes at the comparably low strain rate fringes of tectonic plate boundaries. We illustrate how robust paleoseismic information for long-recurrence interval faults with diffuse and complicated patterns of surface rupture can be obtained by combining subsurface displacement measurements with multi-method high resolution surface displacement measurements.

2. Tectonic, geologic and geomorphic settings

The Greendale Fault sits at the eastern periphery of the Pacific–Australian plate boundary deformation zone in New Zealand's South Island (Fig. 1). The Pacific and Australian plates converge obliquely in a west to southwest direction at ~35–44 mm/year (e.g., Beavan et al., 2002; DeMets et al., 2010; Wallace et al., 2007). In the central South Island, slip on the Alpine Fault accommodates ~75% of the plate

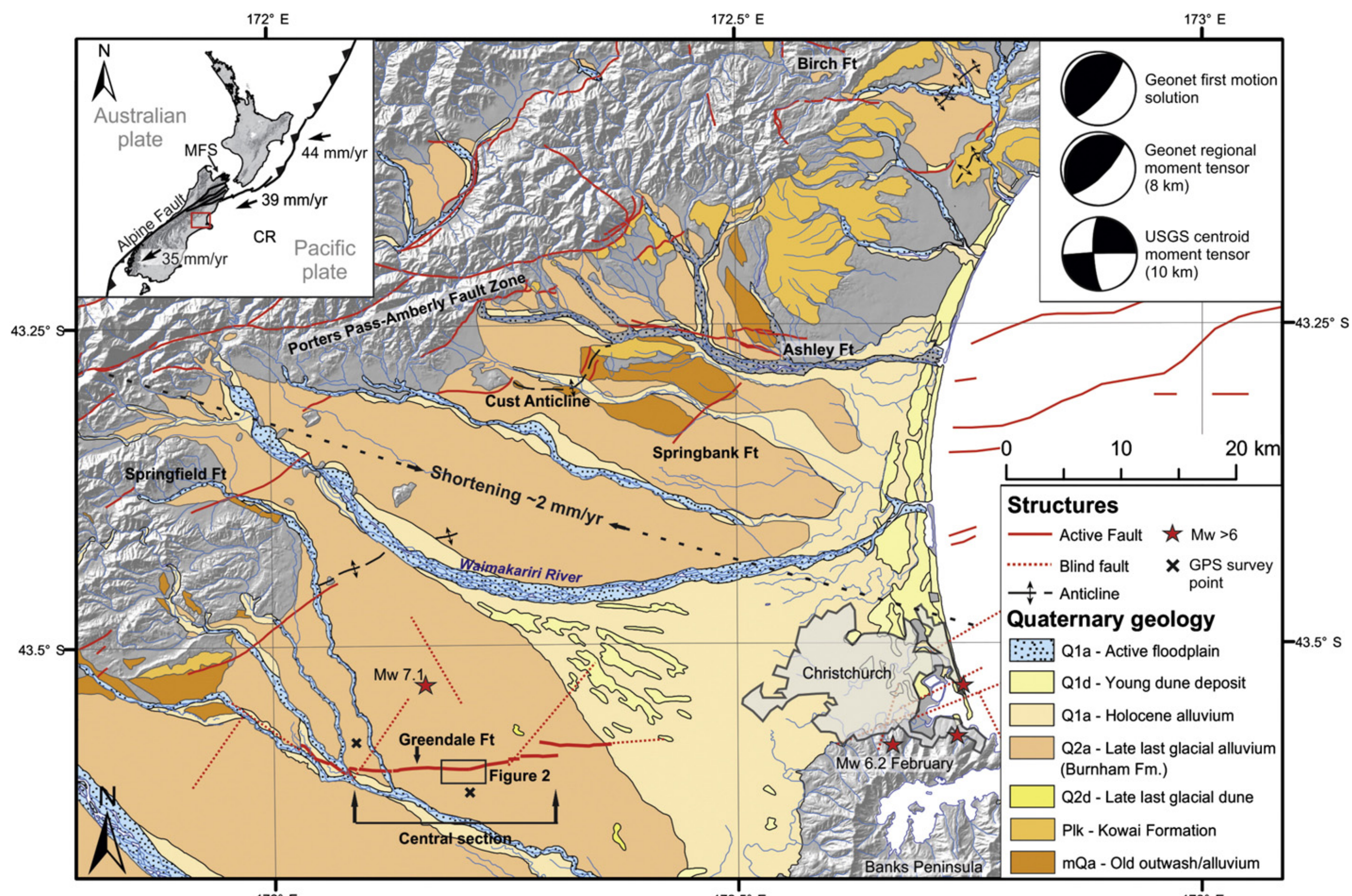

Fig. 1. Location map showing active faults (including the Greendale Fault) and Quaternary deposits (modified from Cox and Barrel, 2007; Forsyth et al., 2008). Gray areas are those largely underlain by Tertiary or older bedrock. Position of blind faults from Beavan et al. (2012) and regional shortening from Wallace et al. (2007). Stars show epicenters of the main events in the Canterbury earthquake sequence. Inset (upper left) shows plate boundary setting and relative motion vectors (DeMets et al., 2010). MFS = Marlborough Fault System; CR = Chatham Rise; location of the study area is shown by the red box. Inset (upper right) shows focal mechanism solutions for the M_w 7.1 September 4, 2010 Darfield earthquake from Gledhill et al. (2011).

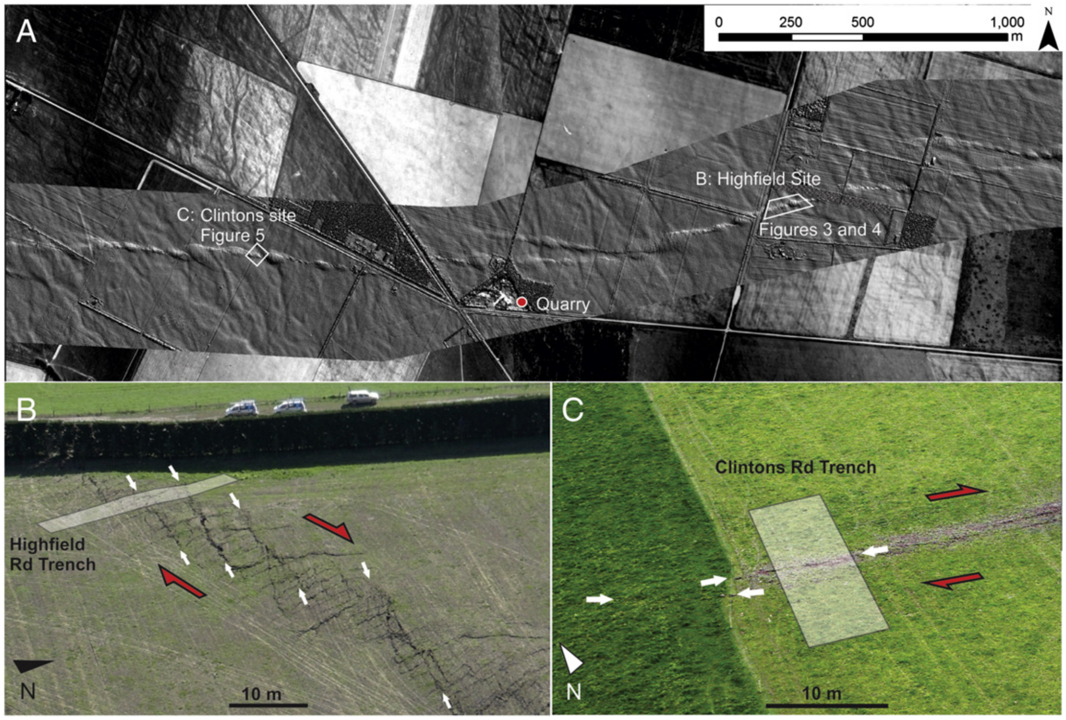

Fig. 2. (A) Central Greendale Fault trace geometry shown via post-rupture lidar over a 1940 ortho-aerialphoto background. Locations of the trench sites are shown. (B) Oblique aerial view of the Highfield Road trench site with Riedel shears highlighted by white arrows. Also visible are antithetic Riedel shears and 'pop-up' structure of fault scarp. Red arrows denote sense of shear. (C) Oblique aerial view of the Clintons Road site with Riedel shears (highlighted by white arrows) offsetting grass verge at the fence line.

convergence and produces uplift of the Southern Alps, with the remainder of the convergence distributed on lower slip rate active faults east of the Alpine Fault (Norris and Cooper, 2001). Few active faults have been mapped at the ground surface in the Canterbury Plains region (e.g., Cox and Barrel, 2007; Forsyth et al., 2008). Geodetic measurements indicate ~2 mm/year regional shortening oriented at ~97° east of the Porter's Pass-Amberley fault zone (Fig. 1) (Wallace et al., 2007). Some of this shortening is converted to permanent strains accommodated by anticlines and related thrusts (e.g., Springbank Fault, Springfield Fault and Cust Anticline; for summary see Litchfield et al., 2014b), oriented subparallel to the Marlborough Fault System along the western edge of the Canterbury Plains (Jongens et al., 1999). Prior to the Darfield earthquake it was considered unlikely that these anticlines and thrusts accommodated all of this shortening, and active strike-slip and reverse faults were inferred to be concealed beneath the Canterbury Plains (Pettinga et al., 2001; Wallace et al., 2007) (Fig. 1). To account for the possibility of large magnitude earthquakes on previously unidentified faults, a M_w 7.2 maximum cutoff has been used for distributed seismicity in the New Zealand National Seismic Hazard Model (Stirling and Gerstenberger, 2010; Stirling et al., 2012).

The Greendale Fault strikes approximately E-W and is inferred to be a reactivated Cretaceous normal fault (Campbell et al., 2012; Davy et al., 2012; Ghisetti and Sibson, 2012; Jongens et al., 2012). Seismic reflection profiles on the Canterbury Plains and the offshore Chatham Rise east of Banks Peninsula show many E-W striking normal faults that mainly accrued displacement in the Late Cretaceous to Paleocene (Browne et al., 2012; Campbell et al., 2012; Davy et al., 2012; Dorn et al., 2010; Field et al., 1989; Ghisetti and Sibson, 2012; Jongens et al., 1999, 2012; Wood and Herzer, 1993). Some of these faults (e.g., Ashley and Birch faults, Fig. 1) have been reactivated in the contemporary stress field (Campbell et al., 2012; Nicol, 1993), which has a WNW-ESE ($115 \pm 5°$) trending regional maximum compressive stress (e.g., Balfour et al., 2005; Nicol and Wise, 1992; Sibson et al., 2012; Townend et al., 2012). This maximum compressive stress orientation is consistent with predominately right-lateral strike-slip on E-W striking faults, as was produced on the Greendale Fault during the Darfield earthquake (Sibson et al., 2011).

The Darfield earthquake and the Canterbury earthquake sequence occurred within ~30 km of thick crust of the Pacific Plate (Eberhart-Phillips and Bannister, 2002). Basement rocks in Canterbury comprise Permian-Early Cretaceous Torlesse Composite Terrane and their metamorphic equivalents at depth. The majority of the events in the Canterbury earthquake sequence occurred in Torlesse basement and the immediately underlying schist. Beneath the Greendale Fault at a depth of 10–12 km these basement rocks are inferred to rest on Mesozoic ocean crust; the Darfield earthquake may have nucleated close to this boundary between continental and ocean crust (Reyners et al., 2014). Basement is unconformably overlain by a 1–2.5 km thick cover sequence of Late Cretaceous-Neogene sedimentary and volcanic rocks (Browne et al., 2012; Field et al., 1989; Forsyth et al., 2008). Unconsolidated to weakly lithified Quaternary sediments and sedimentary rocks form a ~240 m to 1 km thick cover underlying the Canterbury Plains (Brown and Weeber, 1992; Jongens et al., 1999). Earthquakes in the Canterbury sequence are mainly deeper than the cover sequence.

The Greendale Fault displaces the surface of the Canterbury Plains, which were formed by a series of coalescing alluvial fans comprising mainly gravels deposited by the river systems draining the Southern Alps (Alloway et al., 2007; Cox and Barrel, 2007; Forsyth et al., 2008). These Quaternary gravels are inferred to have been mainly deposited as outwash during periods of glaciation. The latest period of gravel aggradation is thought to have occurred during the Last Glacial Cold Period (LGCP) (~28,000 to ~18,000 years ago) and waned in response to glacial retreat in the upper reaches of the main river valleys (Alloway et al., 2007; Forsyth et al., 2008). Alluvial aggradation was followed by down-cutting of the main rivers and, in the region of the Greendale Fault, abandonment of the constructional surface (Cox and Barrel, 2007) (Figs. 1 and 2). The Greendale Fault ruptured through these alluvial outwash gravels, which are locally referred to as the Burnham Formation (Forsyth et al., 2008), for ~80% of its 29.5 km surface-trace length. Exposures of the Burnham Formation indicate that it mainly consists of unconsolidated, moderately well-sorted to very poorly-sorted, moderately- to well-rounded, pebbly to cobbly (clasts < ~20 cm) cm) sandy gravels (typical bedding thickness of gravel deposits is ~1–3 m), with 10–30 cm intercalated lenses of silty sand. Gravel clasts were primarily composed of unweathered and indurated Torlesse greywacke which, in the region of the central Greendale Fault, were transported southeastwards by the ancestral Waimakariri River (Fig. 1).

3. Geometry and slip of the Darfield earthquake rupture

InSAR imagery, GPS measurements and seismicity data indicate that the 4 September 2010 M_w7.1 Darfield earthquake was sourced from a complex rupture comprising multiple faults and fault segments. These structures included E-W striking right-lateral, NE-striking reverse, NNW-striking left-lateral, and NW-striking normal right-lateral faults (Beavan et al., 2010, 2012; Elliott et al., 2012; Holden et al., 2011). Because the earthquake initiated on a steep reverse fault, the first motion solution is reverse (Fig. 1; Gledhill et al., 2011); however, the dominant moment release was sourced from dextral strike slip on the Greendale Fault, as shown by the centroid moment tensor (Fig. 1). Maximum slip of >7 m occurred at 2 to 6 km depth over a 7–8 km strike length on the central Greendale Fault, primarily within Torlesse basement rocks (Beavan et al., 2010, 2012). The combined subsurface rupture length of the three segments of the Greendale Fault is estimated at 48 km (Beavan et al., 2010, 2012). The aftershock sequence following the Greendale Fault rupture shows an eastward propagation of seismicity (Bannister and Gledhill, 2012) with greatest activity in those areas which did not experience maximum slip during the Darfield earthquake (Syracuse et al., 2013). The inferred upper tip-lines of blind faults (Fig. 1) that ruptured in the Darfield earthquake range from 0.5 to 1 km depth (Beavan et al., 2012), suggesting that discrete rupture likely ceased near the base of the Pliocene (~1 km depth) or Quaternary (~0.5 km depth) sedimentary deposits (Jongens et al., 2012). Calculation of Darfield earthquake static stress drop for individual segments range from 6 to 10 MPa (Elliott et al., 2012) to 13.9 $\pm$ 3.7 MPa averaged over the entire Greendale Fault (Quigley et al., 2012). The larger of these estimates is comparable to the ~16 MPa apparent stress calculated for the Darfield earthquake by Fry and Gerstenberger (2011).

The Greendale Fault rupture produced mainly right-lateral displacements across flat grassed farmland (Barrell et al., 2011; Quigley et al., 2010a, 2010b). Mapping of the Greendale Fault at the ground surface took place in the weeks immediately following the earthquake and involved the collection of airborne lidar, RTK GPS survey data, and field measurements of vertical and right-lateral displacement using both tape and compass and RTK (Litchfield et al., 2014a). The intensive agricultural land-use of the Canterbury Plains provided over 100 displaced cultural markers that could be measured with high precision (e.g., roads, fences, crop rows, plow-lines, canals, tree-lines and power-lines). The 29.5 $\pm$ 0.5 km long surface rupture had a maximum right-lateral surface displacement of 5.3 m (Litchfield et al., 2014a; Quigley et al., 2012). In the central section of the fault, at the ground surface, ~70% of the total right-lateral displacement was accommodated by broad-wavelength (10s to 100s of meters) folding about steeply inclined hinges, and only ~30% was accommodated by discrete (faulting) deformation (Quigley et al., 2010a; Van Dissen et al., 2011, 2013). Surface displacements above areas of maximum inferred subsurface slip typically range from 4 to 5 m, indicating a gradual (~1 m per km) vertical decrease in coseismic slip towards the ground surface. This decrease may reflect transfer of confined slip at depth to inelastic deformation accommodated by intergranular sliding in the unconsolidated gravels. Significant strike-slip gradients are observed along the surface fault trace across step-overs and where blind faults that slipped during the Darfield event project to intersect the Greendale Fault (Fig. 1).

The surface trace of the Greendale Fault is segmented over a range of scales from meters to kilometers. At scales of 100 s of meters and less the surface rupture often comprises a series of en-echelon left-stepping segments separated by pop-up structures which form at restraining steps (e.g., Fig. 2A). On a meter to 10s of meters scale, distinctive Riedel (R) and Riedel prime (R′) shears make up the majority of discrete surface deformation and are oriented up to 30° and ~50–70° from the general fault strike, respectively.

4. Fault trenching

4.1. Pre-trenching site investigations

Prior to trenching, the surface and sub-surface structure of small sections of the central Greendale Fault were studied using terrestrial lidar and GPR to aid trench-site selection. Given the abundance of offset cultural features, the Highfield Road site (Figs. 2B, 3 and 4) was the first targeted for paleoseismic investigation. Acquisition of terrestrial lidar data at this site was undertaken immediately following the earthquake (see Litchfield et al., 2014a for data capture and processing details) to characterize surface rupture and folding within the fault deformation zone (Fig. 3A). Lidar data enabled high precision surface displacement measurements to be made at the planned location of the paleoseismic trench. GPR surveys (see Supplementary Information for data capture and processing details) were conducted to determine whether stratigraphy that might form displacement markers was present at the planned Highfield Road trench site. GPR reveals continuous reflectors (marked by dashed white lines in Fig. 3B) that are interpreted as stratigraphic bedding within 5 m of the ground surface, and justified the selection of the Highfield Road site for trenching. A GPR survey conducted on the western side of Highfield Road is also presented in the Supplementary Information accompanying this manuscript, although trenching was not conducted at this location.

The Highfield Road trench is located on a ~500 m long restraining bend along the Greendale Fault (Highfield site, Fig. **2**). The trench site was selected for excavation because the majority of the faulting and folding was confined to a relatively narrow zone (<20 m), which contained well defined Riedel shears that we hypothesized should be identifiable in the trench walls, while the relatively high vertical component of displacement (~0.9 m) offered the prospect of sediment accumulation on the downthrown side of the fault following paleoearthquakes (Fig. 3). In addition, the trench was located close to displaced fences and tree lines that enabled accurate measurement of surface rupture displacement in the 2010 Darfield earthquake (Fig. 4). Displacements of cultural markers at the ground-surface were used to assess whether displacement of paleo-channels exposed in the trench walls could be accounted for by the 2010 event.

A second site adjacent to Clintons Road (Figs. 2C and 5) approximately 2 km west of the Highfield Road site was selected because of the abundance of displaced cultural features immediately adjacent to a paddock where a paleoseismic trench could be situated. GPR and terrestrial lidar were not obtained from this site. The sites' proximity to high-resolution measurements of displaced fence- and plow-lines and the narrow width (<10 m) of the zone of fault fracturing at the ground surface provided constraints on surface displacements that could aid in the interpretation of subsurface displacements (Fig. 5). The presence of paleo-channels at the surface suggested subsurface equivalents might be present that could provide useful markers for measuring fault displacements.

4.2. Paleoseismic trenching methods

The Highfield Road (Figs. 2B, 3 and 4) and Clintons Road (Figs. 2C and 5) paleoseismic trenches were excavated to characterize the near-surface geometry and paleoearthquake history of the central segment of the Greendale Fault. The trenches were excavated in September 2012 (Highfield Road) and March 2013 (Clintons Road) approximately normal to the fault trace to maximum depths of 3–4 m. The trench walls were logged at 1:20 scale and photographed. Stratigraphic units and

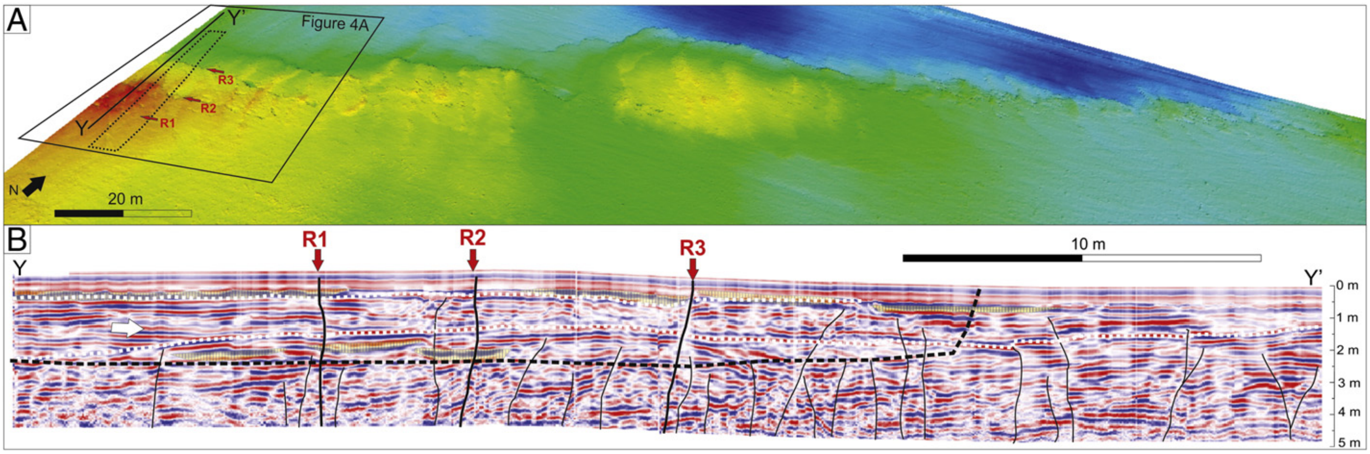

Fig. 3. (A) Terrestrial lidar topographic image of the farm paddock at Highfield Road that contains the trench sites (shown by dashed black line). The data were collected within 1 week of the 2010 Darfield earthquake and capture the main features of the surface rupture deformation zone (see also Figs. 4 and 6). Profile Y-Y′ indicates the location of the GPR profile shown in B. (B) 100 MHz GPR profile that runs along the western wall of the trench. The three major fractures seen at the surface (Riedel shears R1, R2 & R3) were identified, and are marked bold. Many smaller fractures that often do not break through the upper ~1.5 m of the gravel and are only observed in the GPR, not the trench, are identified with black lines. Bold white dashed lines denote continuous reflectors with sedimentary features such as onlap (white arrow) indicating major depositional horizons. Yellow vertically shaded areas over dark reflectors indicate contrasting sandy layers. Approximate outline of the trench excavated at this site (see Fig. 6) is denoted by dashed black line.

structures were described and sandy lenses sampled for OSL dating (Table 1). In four instances, paleo-channels mainly filled with sand or fine gravel were sequentially excavated along the fault strike to record the horizontal and vertical displacements across Riedel shears.

Co-seismic surface displacements generated by the 2010 Darfield earthquake were used to describe the strain distribution across, and to locate the primary fault segments within, each trench. At both trench sites, the total right-lateral displacement is 4.5–5 m and comprises a combination of broad-wavelength folding (distributed deformation) and discrete faulting at length scales of meters to 10s of meters (Figs. 4 and 5). The relative contributions of discrete faulting (about one-quarter to one-third of total strike-slip deformation) and distributed folding (about two-thirds to three-quarters of total strike-slip deformation) are consistent between the two sites. The maximum vertical displacement across the fault zone is ~0.9 m at Highfield Road and <0.2 m at Clintons Road.

4.3. Highfield Road results

The Highfield Road trench was excavated into gravel-dominated alluvial deposits across the entire width of the zone of ground fracturing (Figs. 4 and 6). The stratigraphy comprises stacked cross-bedded fine sand-pebbly gravel beds (20–30 cm thick, with primary stratigraphic dips ranging between 15 and 30°) that are locally separated by sub-horizontal gravel beds. These gravel units contained no paleosols and are overlain by up to 80 cm of silt and silty gravel. Within the gravel-dominated sequence, there are sand-rich lenses of ≥15 cm thickness. These sand lenses often occurred on the margin of cross-bedded gravel sequences and were not laterally extensive indicating that they likely formed as side channels where fine material collected. Six sand lenses were exposed in the west wall of the trench, four of which are located on the downthrown side of Riedel shear R3 (Fig. 6A). The trend of these sand-filled paleo-channels and the imbrication of clasts in the gravel units indicate a general NW to SE paleoflow direction, consistent with the gravels being deposited by the Waimakariri River (Fig. 6A).

Tens of fractures were exposed in the walls of the Highfield Road trench (Fig. 6A). The most prominent structures in the trench walls were the three Riedel shears observed at the ground surface (R1, R2 and R3; Figs. 4 and 6). These shears are spaced at 5–7 m and comprise fault zones up to 0.5 m wide that at their core contain sub-vertical gravel cobbles rotated into parallelism with the fault surface. These shear zones were the only structures that extended from top to bottom of the trench. Two of the three Riedel shears were observed in both walls of the trench (R2 and R3) while the third terminated within the trench (R1; Figs. 4 and 6). In addition to the Riedel shears, numerous fractures, often with no discernible vertical displacement in the trench walls, were recorded in the silt, silty gravel and soil A horizon in the upper 50 to 80 cm of the trench. Some of the secondary fractures restricted to the upper silty layers were oriented parallel to the R′ shears (i.e., the dashed white lines in Fig. 4A), which strike at a high angle of ~50–70° to the general trend of the fault and at a low angle to the trench walls. Using an intermediate orientation between the R and R′ shears, the maximum compressive stress orientation (σ_1) at the trench site of ~118° (Fig. 6B) is comparable to the regional value of 115 ± 5° (e.g., Sibson et al., 2011).

Analogue models with a comparable σ_1 orientation relative to the fault strike and comprising a cohesive talc layer over a loose granular sand layer replicated the fracture pattern observed in the trench walls (Sasnett, 2013). The localization of brittle failure in the upper silty part of the stratigraphic section and for the models in the talc may have occurred because these materials have a higher unconfined compressive strength, and were more cohesive than the underlying loose to slightly compact gravels and sands.

Displacements were measured at the ground surface across the entire surface rupture deformation zone and on individual Riedel shears at the Highfield Road site (Fig. 4). The total right-lateral displacement across the fault, as measured on the fences and tree lines 15–20 m west of the trench, is 4.8 m. Approximately 1.8 m right-lateral was accommodated by the Riedel shears which individually accommodate 0.5 to 0.8 m horizontal displacement and collectively account for about 60% of the total 2.9 m right-lateral displacement encompassed by the trench (see Fig. 4 histogram). The remaining strike-slip displacement within the trench was achieved by brittle failure in the upper silty section (<80 cm depth) and throughout the section by folding associated with inelastic inter-granular slip of gravel clasts in an unlithified/loose sandy matrix. This distributed deformation also accounts for about 70% of the total 0.9 m vertical displacement across the fault zone with the remainder accommodated by approximately 10 cm (down to the north) on each of the three Riedel shears (Fig. 4). The available displacement measurements for the entire fault zone and the R3 Riedel shear indicate slip vectors of 075°/11° and 095°/13°, respectively.

Displacement measurements and OSL dating have been combined to characterize the spatial and temporal distributions of sub-surface slip. R1 and R3 Riedel shears displace sand-filled paleo-channels (Figs. 6

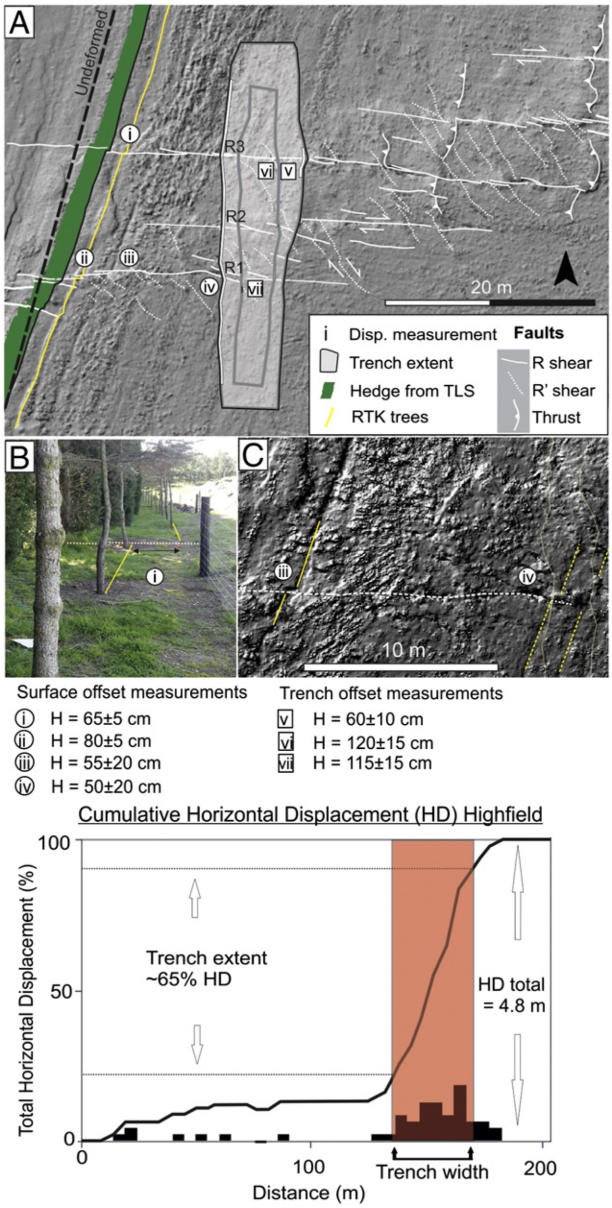

Fig. 4. (A) Highfield Road site map showing Riedel shears (white lines) and Riedel prime shears (dashed white lines), displaced cultural markers, and trench location with lidar image in the background. (B) Photograph of tree row (yellow line in A) where it is displaced by the R3 Riedel shear. (C) A plow-line (offset "iii") and subtle tire tracks (offset "iv"), visible in close up of laser scan, are used for estimating offset measurements at the trench. (D) Plots of cumulative and incremental (histogram) horizontal displacement distribution along the roadside and fence immediately west of the hedge. Bin width is 5 m from field measurement. The trench is located across the highest lateral displacement gradient at the site and its extent is highlighted by the red shading on the cumulative displacement curve. Left lateral steps occasionally occur due to either left lateral offset on Riedel prime shears, or pre-existing deviations in cultural markers. The trench spans ~65% of the total 2010 Darfield earthquake right-lateral displacement at the site (4.8 m), and lateral surface offset on Riedel shears at the site accommodates only about 1/3 of the total lateral displacement.

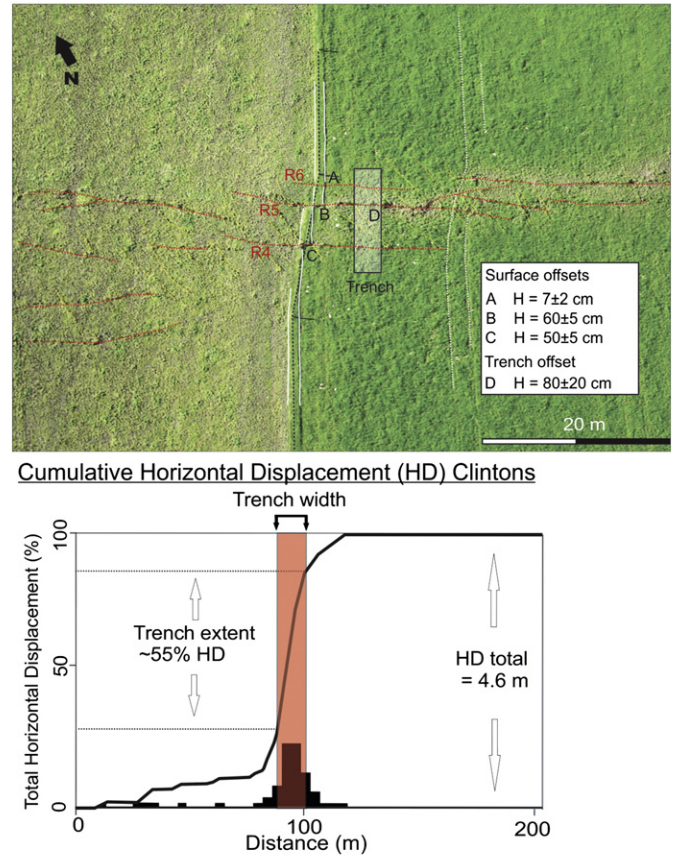

Fig. 5. Clintons Road site map of 2010 ground-surface rupture and displaced features on background of post-rupture air-photo. Black dashed line denotes offset fence, and white solid lines on either side denote offset plow-lines. Dashed white lines show tire tracks deformed right-laterally across the fault trace. Solid red lines are Riedel shears and dashed red lines Riedel prime shears. Plots of cumulative and incremental (histogram) displacement along the fence line. Bin width is 5 m from field measurement. Right-lateral displacement on discreet structures (Riedel shears) at the site is ~117 cm, which is ~25% of the total 4.6 m strike-slip displacement. The trench is located across the highest displacement gradient at the site, and its extent is highlighted by the red shading on the cumulative displacement curve. The trench spans approximately half (~55%) of the total 2010 Darfield earthquake right-lateral displacement at the site.

and 7) that trend at a high angle to the fault ($\geq \sim 70°$) and thus provide piercing points for measuring displacement. Along-strike excavation of the upper section of R3 revealed that the eastern margin of an upper sand lens (see layer including sample OSL 1) was displaced by 60 cm ± 10 cm (horizontal) and 9 ± 5 cm (vertical) (Fig. 7A). Displacement uncertainties reflect the presence of irregularities on the channel margin and its projection into the fault by ~10 cm. The 60 ± 10 cm right-lateral offset is within error of the 65 ± 20 cm RTK and tape-and-compass measurements of an offset tree line cut by the same (R3) shear 18 m to the west (Fig. 4B) and similar to lateral displacements measured on the nearby R1 Riedel shear. The similarity of displacements on the R3 shear for the paleo-channel and cultural features suggests that the only earthquake to rupture this shear at the ground surface occurred during the 2010 Darfield earthquake. Therefore, the age of the displaced paleo-channel provides a minimum age for the penultimate surface-rupturing earthquake on the R3 shear at the trench site. OSL 1 (Fig. 6C) yielded an age for this paleo-channel of 21.6 ± 1.5 ka (Table 1).

Displacements were also measured for two channels deeper in the section and within the oldest exposed sedimentary unit in the trench (see Fig. 7B and C). The channel in the lower east wall (see sample OSL 6) was displaced by R3 and the channel in the lower west wall (see sample OSL 3) by R1. The axis of the channel displaced by R3 contained a distinctive 18 cm thick silt lens that has been displaced by 120 cm ± 15 cm horizontally and 21 ± 5 cm vertically (Fig. 7B). Similarly, the western edge of the sand-filled paleo-channel close to the base of the trench (Fig. 6A and 7C, see sample OSL 3) is displaced by R1 115 cm ± 10 cm horizontally and 20 ± 5 cm vertically. OSL samples 3 and 6 (Fig. 6A and C) yielded ages of 33.0 ± 2.0 ka and 28.4 ± 2.4 ka, respectively (Table 1). An additional paleo-channel at a similar stratigraphic level (2 m depth, OSL 4; Fig. 6) yielded an age of 32.1 ± 1.8 ka

Table 1
Summary of OSL samples collected at the trench and quarry sites located in Fig. 2. Analytical details and radial plots for OSL optical age derivations are provided in the Supplementary Information.

Site	Location (NZTM)	Laboratory number[‡]	Field number	Depth (m)	Water %	Total dose rate (Gy/Ka)	Equivalent dose (Gy)	Optical age (ka)[†]
Highfield	N5172880	WLL1048	OSL 1	0.55	10.5	3.59 ± 0.16	77.58 ± 3.65	21.6 ± 1.5
	E1537010	WLL1049	OSL 3	2.7	19.6	3.30 ± 0.19	108.75 ± 2.62	33.0 ± 2.0
		WLL1050	OSL 4	0.95	21.6	2.66 ± 0.14	85.27 ± 1.97	32.1 ± 1.8
		WLL1051	OSL 6	2.2	9.5	3.70 ± 0.14	104.17 ± 7.74	28.4 ± 2.4
Clintons	N5172701 E1535117	WLL1087	T21	1.6	4.7	4.06 ± 0.14	130.98 ± 7.00	32.3 ± 2.1
Quarry	N5172667	WLL1097	TCP1	4	14.1	4.17 ± 0.22	89.15 ± 3.90	20.2 ± 1.9
	E1536137	WLL1098	TCP2	1	10.7	3.62 ± 0.16	84.43 ± 6.59	24.7 ± 1.5

‡ All samples analyzed at the Victoria University of Wellington OSL laboratory with measurements taken of blue luminescence from fine-grained feldspar produced during infrared stimulation.
† All ages for the single aliquot regeneration method (Wang, 2013), reported with 1 sigma uncertainties.

and is within one-sigma error of both the OSL 3 and 6 ages. Given these OSL dates and their uncertainties the age of the oldest displaced paleochannels is estimated to be about 30 ka.

The displacements of the oldest channels on R1 and R3 are approximately double the displacement of the culture markers at the ground surface and, in the case of R3, the offset of the paleo-channel dated by OSL 1 (Fig. 8). The observed up-sequence changes in displacement could be explained by high vertical displacement gradients during a single rupture or by the stratigraphy lower in the trench having experienced multiple earthquake displacements. Given the small (~1 m) distance between the variably displaced beds and the lack of a displacement decrease above the OSL 1 lens, we favor the multiple event interpretation. This is considered further in the Greendale fault penultimate event and recurrence intervals section.

4.4. Clintons Road results

The Clintons Road trench exposed gravels similar to those at Highfield Road; however, no sand lenses useful for OSL dating and displacement analyses were observed (Fig. 9). The gravel-dominated units at Clintons Road, like those at Highfield Road, comprised alternating cross-bedded units and sub-parallel horizontal units with an absence of paleosols. Imbrication of gravel clasts outside of shear zones indicates paleoflow directions towards the southeast, consistent with the local trend of paleochannels. One of these channels crosses the northern end of the trench and is filled with silt up to ~20 cm thick (Fig. 9A). The gravel units below the silt are subdivided based on changes in primary stratigraphic bed dip, clast size and sand content.

At the Clintons Road trench, the fault strikes almost E-W and is expressed as a series of three left-stepping Riedel shears spaced at 3 and 6 m (labeled R4, R5 and R6 in Fig. 5). These shears are accompanied by R′ shears that trend at 50° to the Riedel shears. The Riedel shears produce a number of small (~20 m across, ~0.5 m high) push-up structures at restraining stepovers (Fig. 2). The R4 and R5 Riedel shears were mapped to the base of the trench at ~3 m depth. The expression of the Riedel shears in the subsurface here was very similar to that of the Highfield Road trench, although without any fine-grained units, discrete fault displacements were more challenging to identify and measure. Both the R4 and R5 Riedel shears were observed in the west wall of the trench; however, only R5 could be mapped in the trench's east wall (Fig. 9C). In the trench walls, these shears (R4 and R5) were marked by zones up to ~30 cm wide containing clasts that had been rotated from their deposition orientations and, in the central ~10 cm of these zones, had long axes parallel to the sub-vertical shear planes

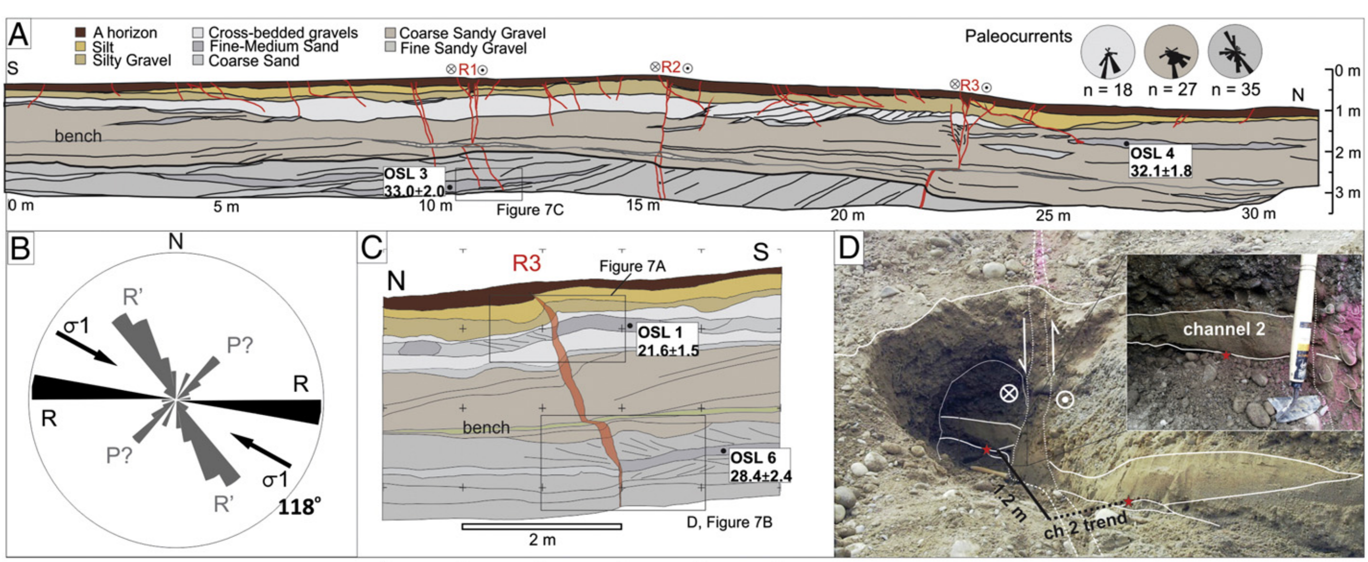

Fig. 6. (A) Log of the west wall of the Highfield Road trench. OSL sample locations are marked. Riedel shears (R1, R2 and R3 are labeled) and fractures are shown by the red lines. Paleocurrent directs measured from various units exposed in the trench with color coding of paleocurrent rose diagram matching colour coding of trench unit lithology. Note 1.5 m wide bench halfway down which appears to offset some features. This bench was installed for safety reasons. (B) Azimuth of fracture planes recorded in the trench. Riedel shears are shown in black with distribution of Riedel prime and other fracture planes (possibly P shears) in gray. (C) Log showing the R3 Riedel shear in the east wall of the trench; key for stratigraphic units is the same for the west wall and locations of OSL are shown. (D) Excavation of the trench wall (location shown in C) to measure offset of sand lens across R3 Riedel shear using piercing point of a gravelly layer at the base of the sand lens. Inset shows appearance of fault at offset edge of sand. Note gravel clasts dragged into sand along the R3 shear, with long axes near-horizontal in slip direction.

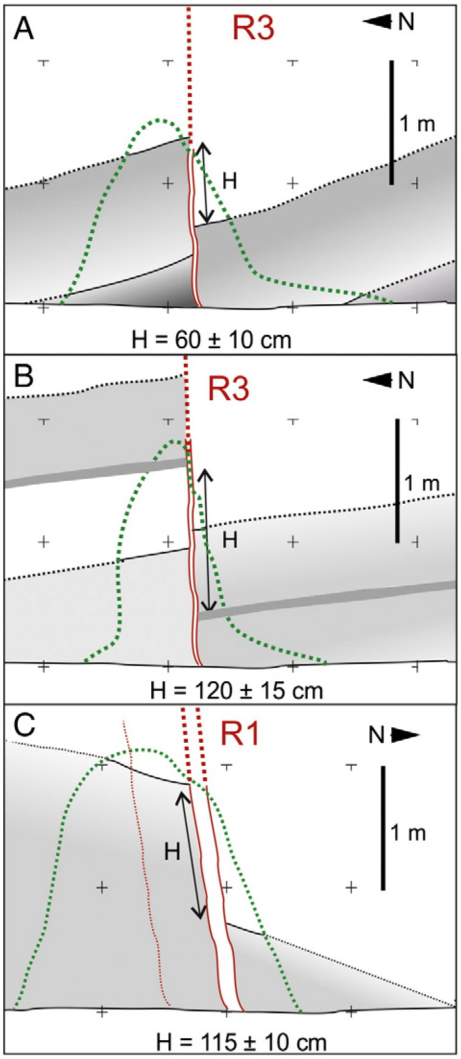

Fig. 7. Highfield Road trench strike-slip displacements shown in map view. Maps were plotted using incremental excavation with limits of the excavation shown by dashed line. Observed contacts are in bold with inferred contacts dotted. (A) Detail of 'single' offset eastern margin of sand channel in upper east wall. Location shown in Fig. 6C. (B) 'Double' offset marker in sand and silt channel in lower east wall. Location in 6C. The piercing point used is marked as a dark gray line and represents a silt-rich area at the channel thalweg which truncated a fine gravel lens in the unit below. (C) 'Double' offset of western channel edge of sandy channel shown in Fig. 6A.

(Fig. 9B and D). In the upper 1 m of the west wall of the trench, R5 was also characterized by a mixed zone of randomly oriented cobbles and soil which we interpret to be fissure fill. In contrast to the Highfield Road trench, discrete R′ shears were not observed in the trench walls near to the surface, possibly due to the lack of the higher compressive strength silt and silty gravel units below ~30 cm depth in this trench.

Displacements were measured across the entire fault zone and on individual Riedel shears mainly using RTK GPS and tape measurements from a fence-line (and associated plow lines) 4–8 m west of the trench. The total right-lateral displacement across the fault deformation zone is 4.6 m and was measured over ~120 m width perpendicular to the fault strike. Approximately 1.8 m right-lateral displacement was accommodated by the Riedel shears which account for about 25% of the total right-lateral displacement, slightly lower than at Highfield Road where the discrete shear accommodates ~35% of the total right-lateral displacement. Of the total right-lateral displacement, approximately 55% was encompassed by the 33 m long trench (see histogram in Fig. 5). Similar to Highfield Road, the high H:V displacement (20:1) on each Riedel shear meant apparent vertical offsets on cross beds in the trench were most likely a result of the dip of the strata, and actual vertical displacement was very small. Vertical displacement at the site is only 15 cm and approximately 10 cm of this was observed on the discrete Riedel shears.

Discrete lateral displacements on the R4 and R5 Riedel shears at Clintons Road resulting from the 2010 Darfield earthquake are similar to those measured at Highfield Road. The R4 and R5 shears displace the fence and plow lines by 50 ± 5 and 60 ± 5 cm respectively (Fig. 5); however, in the absence of terrestrial lidar coverage at the site and poorer quality aerial photography than at Highfield Road, no reliable estimates of ground surface offset were possible at the location of the trench walls. It was however possible to measure sub-surface displacement of one piercing point where it crosses the R5 Riedel shear in the east wall of the trench. Careful excavation into the wall of the trench revealed a ~15 cm thick pea-gravel lens at 2.5 m depth with a northern margin that was right-laterally displaced by 80 ± 20 cm across R5 at this location (Fig. 9D and E). The low angle of the bed orientation to the shear coupled with frequent collapse of the granular material made accurate measurement difficult, hence the comparatively large uncertainties. Given the uncertainties in displacement of the pea gravel and the possibility that displacement of the fence (60 ± 5 cm on R5 at the ground surface) may not represent displacement on R5 at the eastern trench wall (the fence is ~7 m west of the trench wall), it remains uncertain whether displacement of the pea gravel occurred in one or more surface-rupturing earthquakes. An OSL sample (T21) was collected from a gravelly sand approximately 2.5 m below the ground surface (Fig. 9D). It yielded an age of 32.3 ± 2.1 ka (Table 1) that is within error of the OSL ages from the lower parts of the Highfield Road trench. We have less confidence in this age compared to the other OSL ages because it has significant over dispersion caused by individual equivalent dose measurements that vary significantly from the mean equivalent dose (see radial plots in Supplementary Information). The challenges in interpreting offset measurements and sediment ages in this trench reduce our confidence in deriving a robust paleoseismic interpretation here, and we thus place higher value on the data obtained from the Highfield Road trench.

5. Greendale fault penultimate event and recurrence intervals

Following the Darfield earthquake, questions were raised about how many destructive earthquake sources remain undetected close to New Zealand's main cities and how often these sources generate large magnitude earthquakes. The Canterbury earthquake sequence revealed a number of previously unrecognized active faults, but the slip rates and recurrence intervals on these faults remain largely unresolved. For the Greendale Fault the absence of a clear pre-2010 trace on the Canterbury Plains mapped as Burnham Formation (Villamor et al., 2011) suggests that the penultimate surface-rupturing earthquake predates the formation of the Burnham surface at ~16–18 ka (Forsyth et al., 2008), a conclusion that is supported by this study.

While coseismic displacement at depth commonly exceeds surface rupture displacement in major earthquakes, the change in slip with depth is typically low (~1 m/1–2 km) (Beavan et al., 2010). In the case of the R3 Riedel shear at Highfield Road (Figs. 4, 6, 7 and 8), a 50% reduction in displacement occurs over ~1.5 m stratigraphic depth (distance between sand lenses dated by OSL 1 and OSL 6); however, there is no apparent decrease in displacement between the OSL 1 lens and the ground surface ~60 cm above. The strike-slip displacement gradient for the R3 Riedel shear between the dated sand lenses is 0.4 (i.e. 60 cm displacement decrease in 1.5 m) which is several orders of magnitude greater than the average slip gradient of ≤0.001 (m/m) estimated from geodetically-derived rupture models for a maximum strike-slip of 7 m at a depth of 2 km and 5 m at the ground surface (Beavan et al., 2010). In addition, we observe no evidence of the R1 and R3 Riedel shears bifurcating up-sequence in the trench or transferring displacement to new structures in the upper section of the trench stratigraphy.

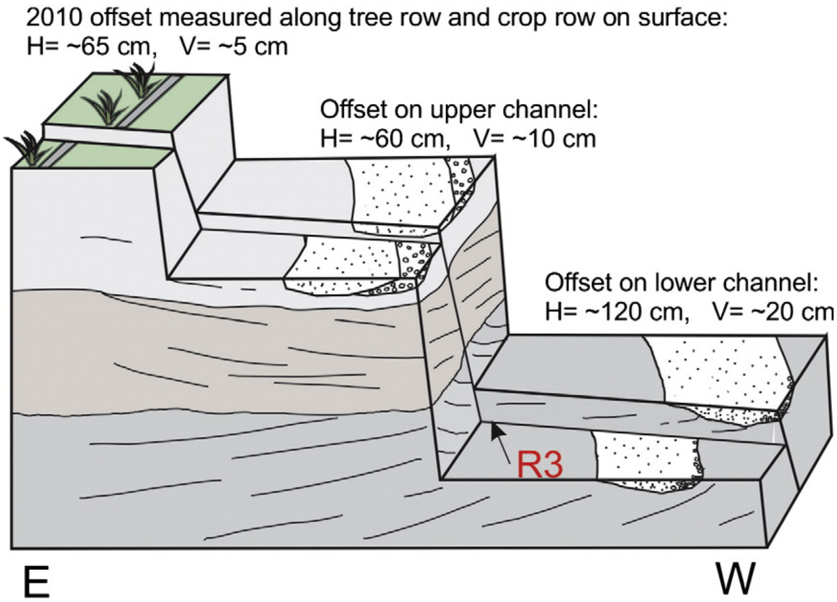

Fig. 8. Schematic block diagram showing displaced paleo-channels across R3 Riedel shear at Highfield Road. Layer colors are the same as used in the trench log (Fig. 6).

For these reasons we do not favor using a single event to explain the observed up-sequence decrease in displacement. Currently our preferred interpretation is that older stratigraphy in the Highfield Road trench has experienced a surface-rupturing earthquake in addition to the 2010 event.

If the multiple-event hypothesis is correct, then the ages of the sand lenses that fill the paleo-channels displaced by one and two earthquakes constrain the timing of the penultimate event on the fault. Therefore, OSL 1 and OSL 3, and 4 and 6 samples bracket the timing of the penultimate event on the Greendale Fault. These sand lenses have ages of 21.6 ± 1.5 ka (OSL 1) and ~30 ka (OSL 3, 4 and 6) (Table 1, Fig. 10). Taking into account the one sigma uncertainties on the OSL 1 age and our best estimate of the older sand lenses the penultimate event on the Greendale Fault most likely occurred between ca. 20 and 30 ka. Angular discordance at an erosional contact was noted in the trench <0.8 m above OSL 3 and OSL 6 sand lenses (see thick lines in Fig. 6A and C), but with the uncertainties on the OSL dates the erosional contact cannot be demonstrated to represent a significant break in time. Given the lack of confidence in assigning a location of an event horizon in the trench stratigraphy, we do not attempt to further refine the timing of the penultimate earthquake age with numerical modeling.

As we only have displacement data for the penultimate event on two Riedel shears at one site where the fault zone is both diffuse and complex, the magnitude of this event remains poorly constrained. Because the postulated earthquake on the Greendale Fault between 20 and 30 ka ruptured the ground surface, and historical surface-rupturing earthquakes on reverse and strike-slip faults in New Zealand (i.e. post 1840) were rarely less than M_w 7 (Nicol et al., 2012), the penultimate

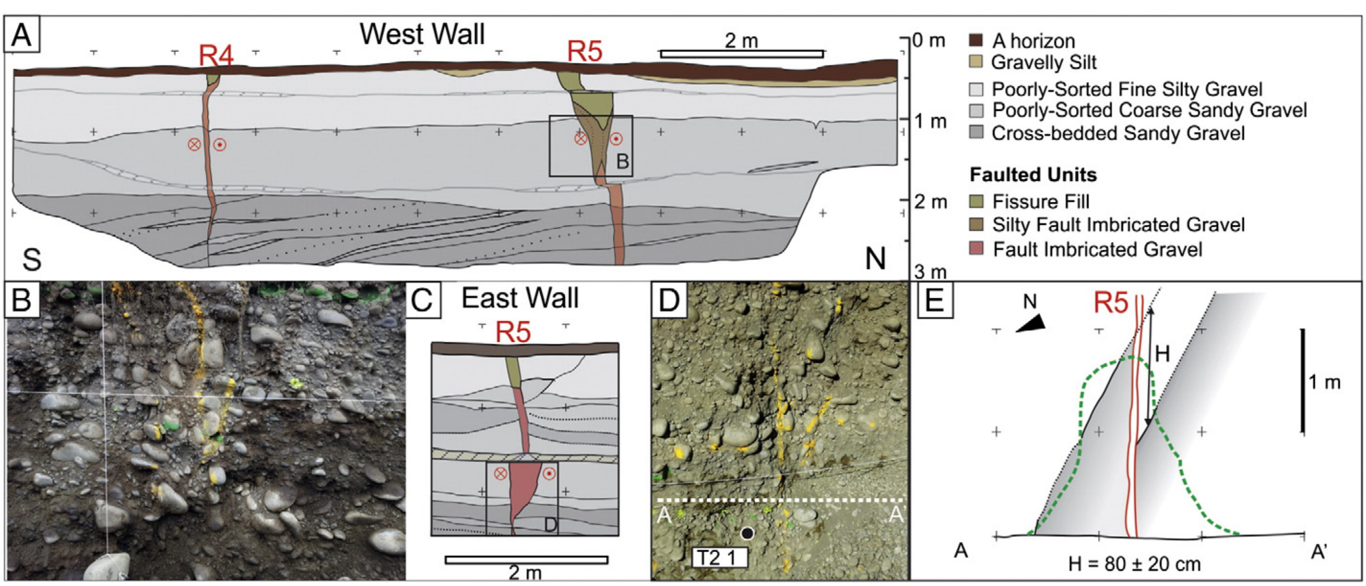

Fig. 9. Clintons Road site trench. (A) Log of west wall of trench showing Riedel shears and layered gravel stratigraphy. (B) Fault imbricated gravel clasts showing clast rotation increasing into fault zone (orange spray paint) where their long axes are sub-vertical. (C) Detail of east wall showing multiple sandy gravel layers across the R5 Riedal shear which has variable width. (D) Photo of 'pea gravel' layer in the lower wall (see C for location) that was used for offset measurement, and OSL sample location (T21) in gravelly sand immediately below this. (E) Map view of section A–A′ showing the 80 ± 20 cm strike-slip displacement of the northern margin of the channel filled with pea gravel in (D). Map was plotted using incremental excavation with limits of the excavation shown by dashed line. Observed contacts are in bold with inferred contacts dotted.

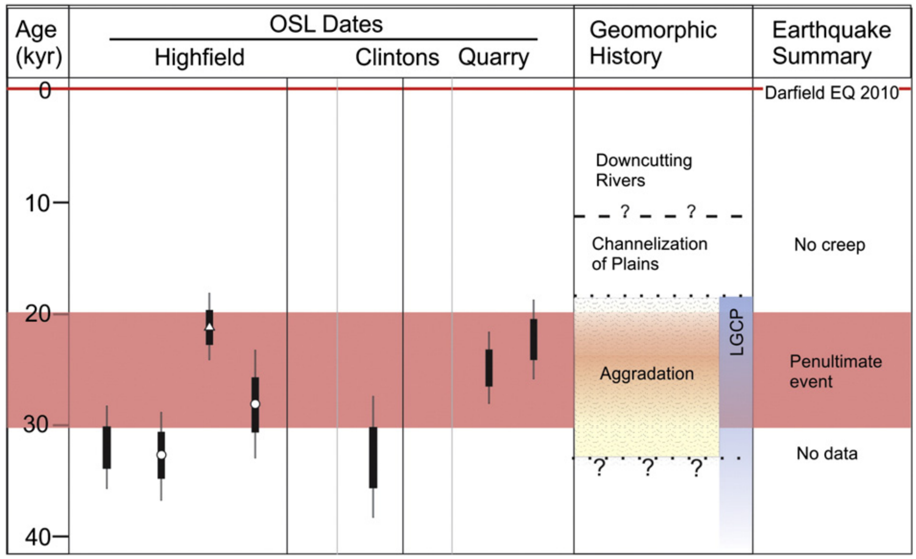

Fig. 10. Summary of OSL ages with 1 sigma (black rectangle) and 2 sigma (line) error bars for stratigraphy at each trench site. White filled circles denote paleo-channels displaced by two or more surface-rupturing earthquakes and white filled triangle by paleo-channel displaced by only the 2010 Darfield earthquake. Red polygon shows preferred timing of the penultimate event.

event was most likely $\geq M_w$ 7. The consistency between the penultimate and most recent displacements on the R1 and R3 Riedel shears in the Highfield Road trench suggests that the penultimate surface-rupturing earthquake had a similar displacement at this site to that which occurred during the 2010 Darfield earthquake. If slip distributions along the Greendale Fault during the penultimate earthquake were consistent to those observed in the Darfield earthquake, then it is likely that the penultimate earthquake was similar in magnitude (~ M_w 7.0; Beavan et al., 2012) to the Greendale Fault M_w contribution to the Darfield earthquake. If other blind faults that ruptured in the Darfield earthquake also ruptured during the penultimate earthquake, then the M_w of the penultimate earthquake would have been similar to the Darfield earthquake.

The Greendale Fault has probably ruptured the ground surface repeatedly over geologic timescales. A seismic reflection survey across the Greendale Fault along Highfield Road indicates vertical displacement of ~20 to 30 m for inferred Pliocene sediments at depths of ~300 to 400 m (J. Pettinga and D. Lawton, personal communication 2013). These cumulative subsurface vertical displacements greatly exceed the ~0.4 m average single-event vertical slip at the surface in the Darfield earthquake. Assuming sub-horizontal and relatively planar reflector geometries and vertical slip gradients comparable to those modeled for the Darfield earthquake (Beavan et al., 2012) it is likely that the Greendale Fault ruptured the ground surface in 10s of paleoearthquakes over the last few million years.

6. Discussion

The five dated OSL samples collected from the gravel-dominated alluvial sediments exposed in the Highfield and Clintons Road trenches range in age from 21.6 ± 1.5 ka to 33.3 ± 2.0 ka (Table 1, see Supplementary Information), and provide the first numerical age constraints for this portion of the Waimakariari fan and Burnham Formation. To test the repeatability of these ages, we dated two OSL samples from a nearby gravel quarry (Fig. 2). These samples were collected at 1 m and 4 m depth from sand lenses within gravel-dominated deposits identical to those exposed in the Highfield and Clintons Road trenches, and retuned ages of 24.7 ± 1.5 ka and 20.2 ± 1.9 ka respectively (Table 1). Despite careful testing of these ages, a reason for the age reversal could not be found; however, they are within 2 standard deviations of each other and such age reversals are common in rapidly deposited units (see full discussion of age accuracy in the Supplementary Information). The reliability and regional applicability of OSL ages listed in Table 1 is supported by the age range of 18.2 ± 1.3 to 36.7 ± 2.9 ka for OSL samples in the Burnham Formation 40 km southeast of the Greendale Fault on coastal cliffs (Rowan et al., 2012). Our OSL ages confirm that this portion of the Waimakariri fan was actively aggrading during the LGCP (~18–28 ka) and perhaps as far back as ~35 ka. These dates are compatible with ages previously assigned to the Burnham Formation (e.g., Alloway et al., 2007; Forsyth et al., 2008; Rowan et al., 2012) (Fig. 10).

The long elapsed time between the last two surface-rupturing events on the Greendale Fault, the assumed low slip rates, and the predominance of strike-slip likely promote the poor preservation of the fault at the ground surface. An additional factor contributing to the concealment of the fault was the relative timing of the penultimate surface rupture and alluvial fan aggradation by the Waimakariri River on the Canterbury Plains. Based on OSL dates of the gravel-dominated units exposed in the trenches and the analysis of displacements on the Riedel shears in the Highfield Road trench, the penultimate surface-rupturing earthquake on the Greendale Fault occurred during a period when the alluvial fans were actively building the surface of the Plains (Fig. 10). Under these high energy conditions a fault scarp of 1 m or less in height could be expected to be buried or eroded rapidly. The relative importance of burial and erosion may have varied along the fault trace depending on a number of factors including the scarp height, relief on the fan surface immediately prior to the fault rupture and fluctuations in river bed-load through time. Inspection of the two trenches excavated across the Greendale Fault provide no clear evidence that the fault scarp for the penultimate event survived its encounter with the ancestral Waimakariri River; however, the scarp height was likely small (<1 m) and identifying a scarp in gravel dominated stratigraphy may not be straight-forward.

Displacement on the central Greendale Fault is dominated by broad wavelength folding (termed "horizontal flexure" in Van Dissen et al., 2013) (see Figs. 4 and 5). By trenching a historic rupture with highly accurate surface displacement data from lidar, RTK GPS, and field tape and compass measurements, we provide detailed analysis of the distribution of total offset into different forms of displacement. Displacement on Riedel shears at the two trench sites made up only a quarter to a third of total displacement, despite the fact that both trenches were selected because shear strains were focused into relatively narrow zones compared to adjacent sections along the fault. These observations have two possible implications for paleoseismic studies of active faults that cut through thick (>100 m) unconsolidated Quaternary sediments. First, in these sedimentological settings, trenches 10–20 m in length may only sample part of the fault zone and could miss key components of the deformation field. Second, exceptional preservation of geomorphic displacement markers will be required in the geological record to accurately describe the width of the fault zone and the distribution of displacement within this zone. Potential difficulties in recognizing and accurately mapping displacements across such active fault zones could lead to underestimates of the total and average displacements on the fault. Dolan and Haravitch (2014) discuss the difference between offset on discrete structures versus distributed deformation with implications for underestimation for paleoearthquake displacement and magnitude. The wealth of accurate offset data from lidar and ground based RTK measurement of almost totally straight anthropogenic markers (power poles, paddock fences, roads), directly compared with trenching of the fault, allow for unprecedented data collection and new insight into this problem. The data show a clear dichotomy between what we know about the magnitude of historic surface rupture and what we are able to discern of the modern surface rupture in a carefully excavated and located trench.

The 2010 Darfield M_w 7.1 earthquake is an example of a growing list of events worldwide that rupture faults that were not previously known to exist. In New Zealand, for example, in the post 1840 AD time interval 40–60% of shallow (<30 km) historical earthquakes of magnitude 7 or greater occurred on faults that have been sufficiently well mapped using modern techniques to show that they are capable of generating large magnitude events (Nicol et al., 2011). Given these sampling issues the size of the hazard represented by these unsampled faults and the ability of background seismicity models to account for these hazards remain uncertain. Reducing these uncertainties will be a focus of future seismic hazard research.

Accurately determining the seismic hazards for Christchurch city requires an improved understanding of the number and locations of these possible large earthquake sources (i.e., active faults). Given the large size of the Canterbury Plains (7500 km^2) (Browne and Naish, 2003) and the current expense of collecting sub-surface information (e.g., seismic reflection profiles), it will be challenging to identify and map all of the concealed structures in the next 10–20 years. Comparison of regional GPS strain data and displacement during the Darfield earthquake provides a means of estimating the possible number of Darfield size earthquakes over the last 16–18 kyr (i.e., the timing of abandonment of the Canterbury Plains alluvial fan surfaces). Wallace et al. (2007) indicate a rate of convergence across the Canterbury Plains block, east of Porters Pass to Amberley Fault Zone (see Fig. 1 for location), of about 2 mm/year trending at 115 ±5°. Beavan et al. (2012) document ~3000 mm of ESE shortening across the Greendale Fault during the Darfield event (between the GPS survey points shown in Fig. 1), which at 2 mm/year represents 1500 years of accumulated strain. Assuming that the rates of GPS shortening apply to the long-term and that these strains will mainly be converted to permanent strain during large magnitude earthquakes, up to 12 earthquakes accommodating the same amount of ESE contraction incurred during the Darfield earthquake would be required every ~18 kyr. Geological mapping prior to 2010 revealed few active faults on the Canterbury Plains. From this it might be concluded that much of the 2 mm/year identified in the GPS signal is accommodated in the foothills along the western margin of the Plains and/or on structures beneath the Plains that do not rupture the ground surface and have sufficiently low slip rates such that they do not produce topographic relief. For example, two moderate historical earthquakes (M_w 4.7–4.9 Christchurch; M_w 5.6–5.8 Lake Ellesmere) occurred in the Plains area on unknown faults in 1869 and 1870 (Downes and Yetton, 2012) and similar events could accommodate small portions of the total strain budget identified by the GPS. It is clear that significant gaps still exist in our understanding of active faulting in this region.

7. Conclusions

1. The previously unknown Greendale Fault ruptured the ground surface in the September 2010 moment magnitude (M_w) 7.1 Darfield Earthquake producing a fault zone up to 300 m wide that comprised both distributed (folding) and discrete (faulting) deformations dominated by right-lateral displacement.
2. Discrete surface fracturing accommodates an average of ~30% of the total right-lateral displacement with the remainder taken up by broad wavelength folding about vertical hinges accompanied by a slip between gravel clasts.
3. Comparison of Riedel shear displacement of buried paleo-channels with displacement of agricultural markers (e.g., fences, roads and plow lines) suggests multiple surface rupturing earthquakes on the Greendale Fault.
4. Optically stimulated luminescence (OSL) dating of paleo-channels with factor-of-two differences in strike-slip and vertical displacements suggests that the penultimate surface rupturing event on the fault probably occurred between ~20 and 30 ka.
5. The Greendale Fault remained undetected prior to the Darfield earthquake because the penultimate fault scarp was eroded and buried during Late Pleistocene alluvial aggradation. Similar, active faults with low slip rates (i.e. lower than the rates of sedimentation or erosion) are likely to be concealed in alluvial settings globally.

Supplementary data to this article can be found online at http://dx.doi.org/10.1016/j.tecto.2014.10.004.

Acknowledgments

This research was funded by the New Zealand Earthquake Commission (EQC) (grant number 6/4/1BIE12/624) and by a GNS Science Sarah Beanland Scholarship (2011) to SH. We thank the landowner Mr Fitzgerald for unlimited access to the Highfield Road paddock, and all the workers and managers of the Clintons Road dairy farm for site access.

References

Alloway, B.V., Lowe, D.J., Barrell, D.J.A., Newnham, R.M., Almond, P.C., Augustinus, P.C., Bertler, N.A.N., Carter, L., Litchfield, N.J., McGlone, M.S., Shulmeister, J., Vandergoes, M.J., Williams, P.W., Anderson, B., Brackley, H., Burge, P., Carter, J., Cochran, U., Cooke, P., Crampton, J., Crouch, E., Crundwell, M., Deng, Y., Drost, F., Graham, I., Harper, M., Hayward, B., Hendy, C., Hollis, C., Hughes, M., Kennedy, D., Kennedy, L., King, D., Mackintosh, A., Manighetti, B., Marra, M., Mildenhall, D., Morgenstern, U., Naish, T., Neil, H., Nobes, D., Page, M., Palmer, A., Prior, C., Rieser, U., Rother, H., Shane, P., Strong, P., Suggate, P., Thomson, J., Tonkin, P., Trustrum, N., Van Dissen, R., Vucetich, C., Wilmshurst, J., Woodward, C., Zondervan, A., 2007. Towards a climate event stratigraphy for New Zealand over the past 30 000 years (NZ-INTIMATE project). J. Quat. Sci. 22 (1), 9–35.

Balfour, N.J., Savage, M.K., Townend, J., 2005. Stress and crustal anisotropy in Marlborough, New Zealand: evidence for low fault strength and structure-controlled anisotropy. Geophys. J. Int. 163, 1073–1086.

Bannister, S., Gledhill, K., 2012. Evolution of the 2010–2012 Canterbury earthquake sequence. N. Z. J. Geol. Geophys. 55 (3), 295–304.

Barrell, D.J.A., Litchfield, N.J., Townsend, D.B., Quigley, M., Van Dissen, R.J., Cosgrove, R., Cox, S.C., Furlong, K., Villamor, P., Begg, J.G., Hemmings-Sykes, S., Jongens, R., Mackenzie, H., Noble, D., Stahl, T., Bilderback, E., Duffy, B., Henham, H., Klahn, A., Lang, E.M.W., Moody, L., Nicol, R., Pedley, K., Smith, A., 2011. Strike-slip ground-surface rupture (Greendale Fault) associated with the 4 September 2010 Darfield earthquake, Canterbury, New Zealand. Q. J. Eng. Geol. Hydrogeol. 44, 283–291.

Beavan, J., Tregoning, P., Bevis, M., Kato, T., Meertens, C., 2002. Motion and rigidity of the Pacific Plate and implications for plate boundary deformation. J. Geophys. Res. B Solid Earth 107 (no. B10) (ETG-19).

Beavan, J., Wallace, L., Samsonov, S., Ellis, S., Motagh, M., Palmer, N., 2010. The Darfield (Canterbury) earthquake: geodetic observations and preliminary source model. Bull. N. Z. Soc. Earthq. Eng. 43 (no. 4), 228.

Beavan, J., Motagh, M., Fielding, E.J., Donnelly, N., Collett, D., 2012. Fault slip models of the 2010–2011 Canterbury, New Zealand, earthquakes from geodetic data and observations of postseismic ground deformation. N. Z. J. Geol. Geophys. 55 (3), 207–221.

Bradley, B.A., Quigley, M.C., Van Dissen, R.J., Litchfield, N.J., 2014. Ground motion and seismic source aspects of the Canterbury earthquake sequence. Earthquake Spectra 30 (1), 1–15.

Bray, J.D., Kelson, K.I., 2006. Observations of surface fault rupture from the 1906 earthquake in the context of current practice. Earthquake Spectra 22 (S2), 69–89.

Brown, L.J., Weeber, J.H., 1992. Geology of the Christchurch Urban Area. In: Reay, M.B. (Ed.), Institute of Geological and Nuclear Sciences.

Browne, G.H., Naish, T.R., 2003. Facies development and sequence architecture of a late Quaternary fluvial-marine transition, Canterbury Plains and shelf, New Zealand: implications for forced regressive deposits. Sediment. Geol. 158 (1–2), 57–86.

Browne, G.H., Field, B.D., Barrell, D.J.A., Jongens, R., Bassett, K.N., Wood, R.A., 2012. The geological setting of the Darfield and Christchurch earthquakes. N. Z. J. Geol. Geophys. 55 (3), 193–197.

Campbell, J., Pettinga, J., Jongens, R., 2012. The tectonic and structural setting of the 4th September 2010 Darfield (Canterbury) Earthquake sequence, New Zealand. N. Z. J. Geol. Geophys. 55 (3), 155–168.

Cox, S., and D.J.A. Barrel (2007). Geology of the Aoraki area, Institute of Geological and Nuclear Sciences 1: 250000 Geological Map. *Lower Hutt, New Zealand*.

Davy, B., Stagpoole, V., Barker, D., Yu, J., 2012. Subsurface structure of the Canterbury region interpreted from gravity and aeromagnetic data. N. Z. J. Geol. Geophys. 55 (3), 185–191.

DeMets, C., Gordon, R.G., Argus, D.F., 2010. Geologically current plate motions. Geophys. J. Int. 181, 1–80.

Dolan, J.F., Haravitch, B.D., 2014. How well do surface slip measurements track slip at depth in large strike-slip earthquakes? The importance of fault structural maturity in controlling on-fault slip versus off-fault surface deformation. Earth Planet. Sci. Lett. 388, 38–47.

Dorn, C., Green, A.G., Jongens, R., Carpentier, S., Kaiser, A.E., Campbell, F., Finnemore, M., Pettinga, J., 2010. High-resolution seismic images of potentially seismogenic structures beneath the northwest Canterbury Plains, New Zealand. J. Geophys. Res. B Solid Earth 115 (no. B11).

Downes, G., Yetton, M., 2012. Pre-2010 historical seismicity near Christchurch, New Zealand: the 1869 Mw 4.7–4.9 Christchurch and 1870 Mw 5.6–5.8 Lake Ellesmere earthquakes. N. Z. J. Geol. Geophys. 55 (no. 3), 199–205.

Duffy, B., Quigley, M., Barrell, D., Van Dissen, R., Stahl, T., Leprince, S., McInnes, C., Bilderback, E., 2013. Fault kinematics and surface deformation across a releasing bend during the 2010 Mw 7.1 Darfield, New Zealand, earthquake revealed by differential LiDAR and cadastral surveying. GSA Bull. 125, 420–431.

Eberhart-Phillips, D., Bannister, S., 2002. Three-dimensional crustal structure in the Southern Alps region of New Zealand from inversion of local earthquake and active source data. J. Geophys. Res. 107.

Elliott, J.R., Nissen, E.K., England, P.C., Jackson, J.A., Lamb, S., Li, Z., Oehlers, M., Parsons, B., 2012. Slip in the 2010–2011 Canterbury earthquakes, New Zealand. J. Geophys. Res. B Solid Earth 117 (no. B3).

Field, B.D., Browne, G.H., Davy, B., Herzer, R.H., Hoskins, R.H., Raine, J.L., Wilson, G.J., Sewell, R.J., Smale, D., Watters, W.A., 1989. Cretaceous and Cenozoic Sedimentary Basins and Geological Evolution of the Canterbury Region, South Island, New Zealand, New Zealand Geological Survey Basin Studies 2. Department of Scientific and Industrial Research, Wellington, New Zealand (94 pp. + enclosures).

Fielding, E.J., Lundgren, P.R., Bürgmann, R., Funning, G.J., 2009. Shallow fault-zone dilatancy recovery after the 2003 Bam earthquake in Iran. Nature 458 (7234), 64–68.

Forsyth, P.J., D.J.A. Barrell, and R. Jongens (2008). Geology of the Christchurch area, Institute of Geological and Nuclear Sciences 1: 250000 Geological Map. *Lower Hutt, New Zealand*.

Fry, B., Gerstenberger, M.C., 2011. Large apparent stresses from the Canterbury earthquakes of 2010 and 2011. Seismol. Res. Lett. 82 (6), 833–838.

Ghisetti, F., Sibson, R., 2012. Compressional reactivation of E–W inherited normal faults in the area of the 2010–2011 Canterbury earthquake sequence. N. Z. J. Geol. Geophys. 55 (3), 177–184.

Gledhill, K., Ristau, J., Reyners, M., Fry, B., Holden, C., 2011. The Darfield (Canterbury, New Zealand) M_w 7.1 Earthquake of September 2010: A preliminary seismological report. Seismol. Res. Lett. 82 (no. 3), 378–386.

Gold, R.D., Stephenson, W.J., Odum, J.K., Briggs, R.W., Crone, A.J., Angster, S.J., 2013. Concealed Quaternary strike-slip fault resolved with airborne lidar and seismic reflection: the Grizzly Valley fault system, northern Walker Lane, California. J. Geophys. Res. Solid Earth 118, 3753–3766.

Holden, C., Beavan, J., Fry, B., Reyners, M., Ristau, J., Van Dissen, R., Villamor, P., Quigley, M., 2011. Preliminary source model of the M_w 7.1 Darfield earthquake from geological, geodetic and seismic data. Ninth Pacific Conference on Earthquake Engineering, Building an Earthquake-Resilient Society, Auckland, New Zealand, Paper 164 (8 pp.).

Jongens, R., Pettinga, J., Campbell, J., 1999. Stratigraphic and structural overview of the onshore Canterbury Basin: North Canterbury to the Rangitata River. Report Prepared for Indo-Pacific Energy Ltd., (Permit PEP38256), p. 31.

Jongens, R., Barrell, D.J.A., Campbell, J.K., Pettinga, J.R., 2012. Faulting and folding beneath the Canterbury Plains identified prior to the 2010 emergence of the Greendale Fault. N. Z. J. Geol. Geophys. 55 (3), 169–176.

Kaiser, A., Holden, C., Beavan, J., Beetham, D., Benites, R., Celentano, A., Collet, D., Cousins, J., Cubrinovski, M., Dellow, G., Denys, P., Fielding, E., Fry, B., Gerstenberger, M., Langridge, R., Massey, C., Motagh, M., Pondard, N., McVerry, G., Ristau, J., Stirling, M., Thomas, J., Uma, S.R., Zhao, J., 2012. The M_w 6.2 Christchurch earthquake of February 2011: preliminary report. N. Z. J. Geol. Geophys. 55 (no. 1), 67–90.

Litchfield, N.J., Van Dissen, R., Sutherland, R., Barnes, P.M., Cox, S.C., Norris, R., Beavan, J., Langridge, R., Villamor, P., Berryman, K., Stirling, M., Nicol, A., Nodder, S., Lamarche, G., Barrell, D.J.A., Pettinga, J.R., Little, T., Pondard, N., Mountjoy, J.J., Clark, K., 2014a. A model of active faulting in New Zealand. N. Z. J. Geol. Geophys. 57 (1), 32–56.

Litchfield, N.J., Van Dissen, R.J., Hornblow, S., Quigley, M., Archibald, G., 2014b. Detailed analysis of Greendale Fault ground surface rupture displacement and geometries. GNS Science Report 2013/18.

McCalpin, J.P., Thakkar, M.G., 2003. 2001 Bhuj-Kachchh earthquake: surface faulting and its relation with neotectonics and regional structures, Gujarat, Western India. Ann. Geophys. 46, 937–956.

Nicol, A., 1993. Haumurian (c.66–80 Ma) half-graben development and deformation, mid Waipara, north Canterbury, New Zealand. N. Z. J. Geol. Geophys. 36, 127–130.

Nicol, A., Wise, D.U., 1992. Paleostress adjacent to the Alpine Fault of New Zealand: fault, vein, and stylolite data from the Doctors Dome Area. J. Geophys. Res. B Solid Earth 97 (B12), 17685–17692.

Nicol, A., Begg, J., Mouslopoulou, V., Stirling, M., Townsend, D., Van Dissen, R., Walsh, J., 2011. Active faults in New Zealand: what are we missing? In: Litchfield, N.J., Clark, K. (Eds.), Abstract Volume, Geosciences 2011 Conference, Nelson, New Zealand. Geoscience Society of New Zealand Miscellaneous Publication 130A. ISBN: 978-1-877480-13-3, p. 79.

Nicol, A., Robinson, R., Van Dissen, R., Harvison, A., 2012. Variability in slip/event and recurrence intervals for large magnitude paleoearthquakes on New Zealand's active faults. GNS Science Report 2012/41 (57 pp.).

Norris, R.J., Cooper, A.F., 2001. Late Quaternary slip rates and slip partitioning on the Alpine Fault, New Zealand. J. Struct. Geol. 23, 507–520.

Oskin, M.E., Arrowsmith, J.R., Corona, A.H., Elliott, A.J., Fletcher, J.M., Fielding, E.J., Gold, P.O., Garcia, J.J.G., Hudnut, K.W., Liu-Zeng, J., Teran, O.J., 2012. Near-field deformation from the El Mayor–Cucapah earthquake revealed by differential LIDAR. Science 335 (6069), 702–705.

Pettinga, J.R., Yetton, M.D., Van Dissen, R.J., Downes, G., 2001. Earthquake source identification and characterisation for the Canterbury region, South Island, New Zealand. Bull. N. Z. Natl. Soc. Earthq. Eng. 34, 282–317.

Quigley, M., Van Dissen, R., Villamor, P., Litchfield, N., Barrell, D., Furlong, K., Stahl, T., Duffy, B., Bilderback, E., Noble, D., Townsend, D., Begg, J., Jongens, R., Ries, W., Claridge, J., Klahn, A., Mackenzie, H., Smith, A., Hornblow, S., Nicol, R., Cox, S., Langridge, R., Pedley, K., 2010a. Surface rupture of the Greendale Fault during the M_w 7.1 Darfield (Canterbury) Earthquake, New Zealand: initial findings. Bull. N. Z. Natl. Soc. Earthq. Eng. 43, 236–242.

Quigley, M., Villamor, P., Furlong, K., Beavan, J., Van Dissen, R., Litchfield, N., Stahl, T., Duffy, B., Bilderback, E., Noble, D., Barrell, D., Jongens, R., Cox, S., 2010b. Previously unknown fault shakes New Zealand's South Island. Eos Trans. AGU 91 (49), 469–470.

Quigley, M., Van Dissen, R., Litchfield, N., Villamor, P., Duffy, B., Barrell, D., Furlong, K., Stahl, T., Bilderback, E., Noble, D., 2012. Surface rupture during the 2010 Mw 7.1 Darfield (Canterbury) earthquake: implications for fault rupture dynamics and seismic-hazard analysis. Geology 40, 55–58.

Reyners, M., Eberhart-Phillips, D., Martin, S., 2014. Prolonged Canterbury earthquake sequence linked to widespread weakening of strong crust. Nat. Geosci. 7 (1), 34–37.

Rockwell, T.K., Klinger, Y., 2013. Surface rupture and slip distribution of the 1940 Imperial Valley earthquake, Imperial Fault, Southern California: implications for rupture segmentation and dynamics. Bull. Seismol. Soc. Am. 103, 629–640.

Rockwell, T.K., Lindvall, S., Dawson, T., Langridge, R., Lettis, W., Klinger, Y., 2002. Lateral offsets on surveyed cultural features resulting from the 1999 Izmit and Düzce earthquakes, Turkey. Bull. Seismol. Soc. Am. 92, 79–94.

Rowan, A.V., Roberts, H.M., Jones, M.A., Duller, G.A., Covey-Crump, S.J., Brocklehurst, S.H., 2012. Optically stimulated luminescence dating of glaciofluvial sediments on the Canterbury Plains, South Island, New Zealand. Quat. Geochronol. 8, 10–22.

Sasnett, P. (2013). Analogue modelling of strike-slip surface ruptures: Implications for Greendale Fault mechanics and paleoseismology, *unpubl. MS thesis*, University of Canterbury, New Zealand.

Sibson, R., Ghisetti, F., Ristau, J., 2011. Stress control of an evolving strike-slip fault system during the 2010–2011 Canterbury, New Zealand, earthquake sequence. Seismol. Res. Lett. 82 (6), 824–832.

Sibson, R.H., Ghisetti, F.C., Crookbain, R.A., 2012. Andersonian wrench faulting in a regional stress field during the 2010–2011 Canterbury, New Zealand, earthquake sequence. Geol. Soc. Lond. Spec. Publ. 367 (1), 7–18.

Stirling, M., Gerstenberger, M., 2010. Ground motion-based testing of seismic hazard models in New Zealand. Bull. Seismol. Soc. Am. 100, 1407–1414.

Stirling, M., McVerry, G., Gerstenberger, M., Litchfield, N., Van Dissen, R., Berryman, K., Barnes, P., Wallace, L., Villamor, P., Langridge, R., Lamarche, G., Nodder, S., Reyners, M., Bradley, B., Rhoades, D., Smith, W., Nicol, A., Pettinga, J., Clark, K., Jacobs, K., 2012. National seismic hazard model for New Zealand: 2010 update. Bull. Seismol. Soc. Am. 102, 1514–1542.

Syracuse, E.M., Thurber, C.H., Rawles, C.J., Savage, M.K., Bannister, S., 2013. High- resolution relocation of aftershocks of the Mw 7.1 Darfield, New Zealand, earthquake and implications for fault activity. J. Geophys. Res. Solid Earth 118 (no. 8), 4184–4195.

Townend, J., Sherburn, S., Arnold, R., Boese, C., Woods, L., 2012. Three-dimensional variations in present-day tectonic stress along the Australia–Pacific plate boundary in New Zealand. Earth Planet. Sci. Lett. 353, 47–59.

Van Dissen, R., Barrell, D., Litchfield, N., Villamor, P., Quigley, M., King, A., Furlong, K., Begg, J., Townsend, D., Mackenzie, H., Stahl, T., Noble, D., Duffy, B., Bilderback, E., Claridge, J., Klahn, A., Jongens, R., Cox, S., Langridge, R., Ries, W., Dhakal, R., Smith, A., Hornblow, S., Nicol, A., Pedley, K., 2011. Surface rupture displacement on the Greendale Fault during the Mw 7.1 Darfield (Canterbury) earthquake, New Zealand, and its impact on man-made structures. Ninth Pacific Conference on Earthquake Engineering. Building an Earthquake-Resilient Society, Auckland, New Zealand, Paper 186 (8 pp.).

Van Dissen, R., Hornblow, S., Quigley, M., Litchfield, N., Villamor, P., Nicol, A., 2013. Towards the development of design curves for characterising distributed strike-slip surface fault rupture displacement: an example from the 4 September, 2010, Greendale Fault rupture, New Zealand. 19th NZGS Geotechnical Symposium, pp. 455–462.

Villamor, P., Barrell, D., Litchfield, N., Van Dissen, R., Hornblow, S., Levick, S., 2011. Greendale Fault: investigation of surface rupture characteristics for fault avoidance zonation. GNS Science Consultency Report 2011-121 (59 pp.).

Villamor, P., Litchfield, N., Barrell, D., Van Dissen, R., Hornblow, S., Quigley, M., Levick, S., Ries, W., Duffy, B., Begg, J., Townsend, D., Stahl, T., Bilderback, E., Noble, D., Furlong, K., Grant, H., 2012. Map of the 2010 Greendale Fault surface rupture, Canterbury, New Zealand: application to land use planning. N. Z. J. Geol. Geophys. 55, 223–230.

Wallace, L.M., Beavan, J., McCaffrey, R., Berryman, K., Denys, P., 2007. Balancing the plate motion budget in the South Island, New Zealand using GPS, geological and seismological data. Geophys. J. Int. 168, 332–352.

Wang, N., 2013. Luminescence Dating Technical Report no. 13/3. Luminescence Dating Laboratory, Victoria University of Wellington, New Zealand.

Wells, D.L., Coppersmith, K.J., 1994. New empirical relationships among magnitude, rupture length, rupture width, rupture area, and surface displacement. Bull. Seismol. Soc. Am. 84, 974–1002.

Wesnousky, S.G., 2008. Displacement and geometrical characteristics of earthquake surface ruptures: issues and implications for seismic-hazard analysis and the process of earthquake rupture. Bull. Seismol. Soc. Am. 98 (4), 1609–1632.

Wood, R.A., Herzer, R.H., 1993. The Chatham Rise, New Zealand. In: Ballance, P.F. (Ed.), South Pacific Sedimentary BasinsSedimentary Basins of the World 2. Elsevier Science Publishers, Amsterdam, pp. 329–349.